UNPUBLISHED PRELIMINARY DATA R-9.

35 p

2 (NASA Order R-9)
(NASA CR-52912; NRL Report 5967)

[redacted]

STARK PROFILE MEASUREMENT OF THE LYMAN-α AND LYMAN-β LINES OF HYDROGEN

CR 52912

R. C. Elton

Plasma Physics Branch
Radiation Division

July 17, 1963 35 p

N65 16481

FACILITY FORM 602

N65 16481 (ACCESSION NUMBER)	(THRU)
35 (PAGES)	1 (CODE)
CR 52912 (NASA CR OR TMX OR AD NUMBER)	25 (CATEGORY)

[redacted]

GPO PRICE $ _____

OTS PRICE(S) $ _____

Hard copy (HC) 2.00

Microfiche (MF) .50

6274005

U. S. NAVAL RESEARCH LABORATORY
Washington, D.C.

CONTENTS

Abstract	ii
Problem Status	ii
Authorization	ii
INTRODUCTION	1
APPARATUS DETAILS	2
Capacitor Bank and Circuitry	2
Shock Tube	3
Vacuum Spectrograph	4
Auxiliary Spectrographs	4
High-Speed Camera	5
Oscilloscopes	6
DESCRIPTION OF EXPERIMENT	6
Development of the High-Density Source	6
Vacuum Spectrograph Operation	12
Auxiliary Spectroscopic Measurements	14
SPECTROSCOPIC THEORY	16
Review of Hydrogen Line Broadening Theory	16
Electron Density Determination from the Visible Continuum Radiation	18
Temperature Determination from a Line-to-Continuum Ratio	21
DATA, ANALYSIS, AND RESULTS	22
Obtainment of the Vacuum Ultraviolet Data	22
Reduction of Data	23
Results and Error Estimates	25
SUMMARY, CRITIQUE, AND CONSIDERATION OF FUTURE EXPERIMENTS	28
ACKNOWLEDGMENTS	29
REFERENCES	30

[redacted]

10995

ABSTRACT

A T-type electromagnetic shock tube [Elton, R.C., Griem, H.R., and Kolb, A.C., J. Opt. Soc. Am. 52:605 (1962)] was used for the detailed study of Stark broadened lines in the vacuum ultraviolet. Measurements of the Lyman-α profile from an optically thin region (0.03 percent admixture of hydrogen in 40 mm-Hg helium) indicated agreement to within 10 percent with recent calculations [Griem, H.R., Kolb, A.C., and Shen, K.Y., Phys. Rev. 116:4 (1959)] which included the broadening effects due to electron impacts, as opposed to the Holtsmark theory which differs by a factor of ~3 on the wings when the theoretical curves are normalized at equal slope. A temperature of $(20.5\pm1.6)10^3$ °K has been determined from a line-to-continuum ratio measurement for helium. Density measurements from the visible continuum gave $N_e = (3.6\pm0.4)10^{17}$. The Rankine-Hugoniot equations predicted $N_e = (4.8\pm1.9)10^{17}$ and $T = (20.0\pm1.0)10^3$ °K from the measured shock velocity. A calculated spectral emissivity of 0.09±0.06 at 1217.7A compares with 0.10±0.02 as found experimentally by adding known amount of hydrogen until saturation occurs. It is thus possible to produce near-blackbody radiation from homogeneous plasmas of controlled optical depths. Such plasmas can possibly be used as intensity standards at other wavelengths in the vacuum ultraviolet by using other gases having strong lines appropriatedly spaced. Similar measurements on the Lyman-β line support these results.

AUTHOR

PROBLEM STATUS

This is a report on one phase of the problem; work is continuing on the general program.

AUTHORIZATION

NRL Problem H01-11
Project RR 002-10-45-5054
Jointly supported by NSF and NASA

Manuscript submitted May 10, 1963.

STARK PROFILE MEASUREMENT OF THE LYMAN-α AND LYMAN-β LINES OF HYDROGEN

INTRODUCTION

Astrophysicists have for many years utilized the techniques of spectroscopy, including the measurement of spectral line profiles, to obtain information about the physical state of the atmospheres of stars. To insure an accurate interpretation of the experimental data obtained, various theories have been invoked which have attempted to associate the observed line profiles with the physical properties, such as temperature or particle density, of the light source. Recent interest in the production of high-temperature plasmas in the laboratory, both for use as a light source and as a possible medium in which to obtain a controlled thermonuclear reaction, has prompted expanded efforts towards the use of spectroscopy and its theoretical interpretations as a probe for studying the physical state of partially ionized gases. In particular, the detailed study of spectral line profiles, i.e., the relationship between intensity and wavelength, often affords a sensitive measurement of the electron density or the ion temperature, and the measurement is quite independent of thermal equilibrium conditions.

To gain confidence in the theory for interpreting line profile data, comparisons must be made between the theory and the experimental data obtained from a light source of known conditions, preferably with a gas such as hydrogen that can be handled accurately and relatively simply theoretically. Such a comparison made with arcs (1,2) on the Hβ line of hydrogen indicated, however, that errors existed which were too large to be accounted for in the experimental techniques. The errors were generally attributed to the failure to adequately account for the Stark effect broadening due to the fields of the electrons in the presence of the ions. An improved impact theory developed by Baranger (3) and Kolb and Griem (4), together with the quasi-static theory corrected for correlation and shielding effects, was applied to various hydrogen lines by Griem, Kolb, and Shen (5) and by Mozer (6). Close agreement with experimental results for Hβ is reported by these authors.

Experimental emphasis has been placed on the Hβ line of the Balmer series, which is Stark broadened by electrons and ions, chiefly because its wavelength of 4861A is in the convenient visible region of the spectrum. However, the first two lines in the Lyman series, namely, Lyman-α and Lyman-β, are particularly interesting because, in addition to being simple lines which can be accurately calculated, the slopes of the wings of the profiles are very sensitive to the additional electronic Stark broadening predicted by the above-mentioned theory. Thus a detailed study of their profiles serves as a direct check on the component of the theory dealing with the lighter, fast-moving electrons (impact theory) compared to that of the heavier and slower ions (quasi-static theory), as well as providing confidence in the calculated wing formulae as used by astrophysicists.

Unfortunately, these lines are difficult to study due to their location in the far ultraviolet (1216A for Lyman-α and 1026A for Lyman-β), and they require vacuum spectroscopic techniques for experimental diagnosis. In addition, their half-widths are very narrow at

Note: An earlier version of this report has been submitted to the University of Maryland as a dissertation in partial fulfillment of the requirements for the degree of Doctor of Philosophy.

electron densities below 10^{18} cm^{-3}, which further complicates the problem of resolving their shapes. For these reasons, no previous attempts have succeeded in determining these profiles under controlled conditions.

The program followed in this experiment consisted of two stages: first, the development of a uniform, highly reproducible light source capable of producing a charged particle density of 10^{17} to 10^{18} cm^{-3}, and second, the generation of an optically thin hydrogen region in this high-density atmosphere from which to obtain the Lyman-α and Lyman-β lines to be studied.

Previous experiments at the U.S. Naval Research Laboratory (7,8) with electromagnetically driven shock waves indicated that the obtainment of the desired conditions was feasible by such techniques. Preliminary studies with different configurations soon showed that the linear shock tube was to be preferred to a radial magnetic compression machine since the skin depth at the relatively low temperatures obtained was too great to allow the formation of the high-current sheath required for an efficient compression. A modified T-type shock tube was developed, and studies were made in the region directly behind the reflected shock front at the end of the tube. Small quantities of hydrogen were contained in the helium atmosphere, and the Lyman-α and Lyman-β studies were made with a McPherson model 240 2-meter normal-incidence vacuum spectrograph. Simultaneously, measurements of the temperature T and electron density N_e were made by measuring the intensity of an optically thin helium line relative to the underlying continuum and by measuring the absolute intensity of the optically thin continuum, respectively, in the visible region of the spectrum. Measurements of the incident shock velocity were made with a streak camera, and values for N_e and T were obtained from idealized shock hydrodynamics (9) and compared with those obtained spectroscopically. Shock arrival time measurements, when correlated with the ideal shock theory, helped to verify the reproducibility from shot to shot.

This report contains a description of the experiments performed, the results obtained, and a comparison of these results with theory. The next section describes the experimental apparatus utilized, while the following (third) section treats the manner in which the experiment was carried out.

A brief review of the theoretical aspects of Stark broadening of hydrogen lines is included in the beginning of the fourth section, followed by a discussion of the theory for the auxiliary measurements of electron density and temperature. The evaluation procedure for the data is described in the fifth section, with the summary, critique, and suggestions for future experiments being reserved for the last section.

APPARATUS DETAILS

Capacitor Bank and Circuitry

The capacitor bank used to deliver the high currents required to power the shock tube has the following characteristics:

Capacitance = 108 μf

Maximum voltage = 20,000 volts

Maximum energy = 22,000 joules

Time to peak current = 3 μsec

Peak current = 1.1×10^6 amperes

Total inductance = 34 mμh

External circuit resistance = 0.003 ohm

Shock tube resistance = 0.008 ohm.

The bank was assembled from fourteen Bosch capacitors of 7.7 μf each, with one enclosed air-gap switch (10) per two capacitors. The current is delivered to the collector plate at the shock tube by twenty-one low-inductance coaxial cables. The seven switches are triggered by a 0.1-μf capacitor, operated at 20 kv, which is controlled by a single air-gap switch closed by overvoltage. The system circuit diagram is shown in Fig. 1.

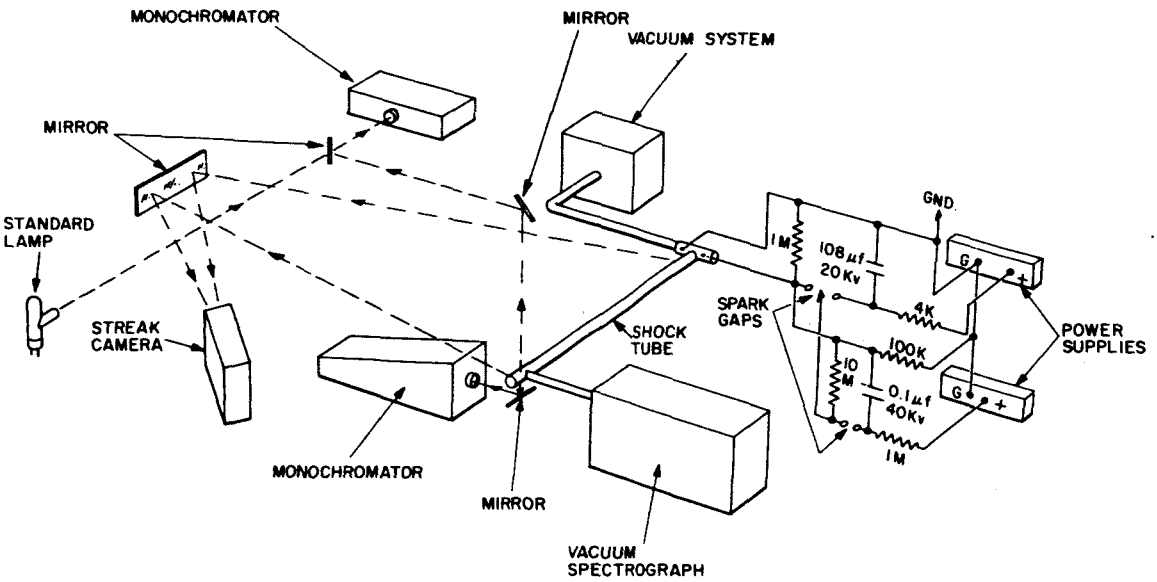

Fig. 1 - Experimental arrangement and circuit diagram

Characteristics of the discharge current are shown in Fig. 2 for both a dummy load and a typical shock tube discharge load. The resistance values given above were calculated from this data; these values show that most of the resistance is in the shock tube. Furthermore, it is apparent that due to the high ratio of C to L as used here, we are close to the condition of critical damping given by

$$R = \sqrt{2L/C} = 0.025 \text{ ohm.} \tag{1}$$

This means that approximately 60 percent of the available energy is dissipated during the important first half cycle when the primary shock wave is formed, implying that succeeding shocks will be greatly reduced in strength without auxiliary "crowbar" techniques.

Shock Tube

The shock tube used, which evolved from a development program outlined in the next section, is shown in Figs. 3 and 4. A 75-cm-long quartz tube, 3-mm wall thickness and 24 mm inside diameter, was used for the longitudinal section with a 9-cm-long cross arm

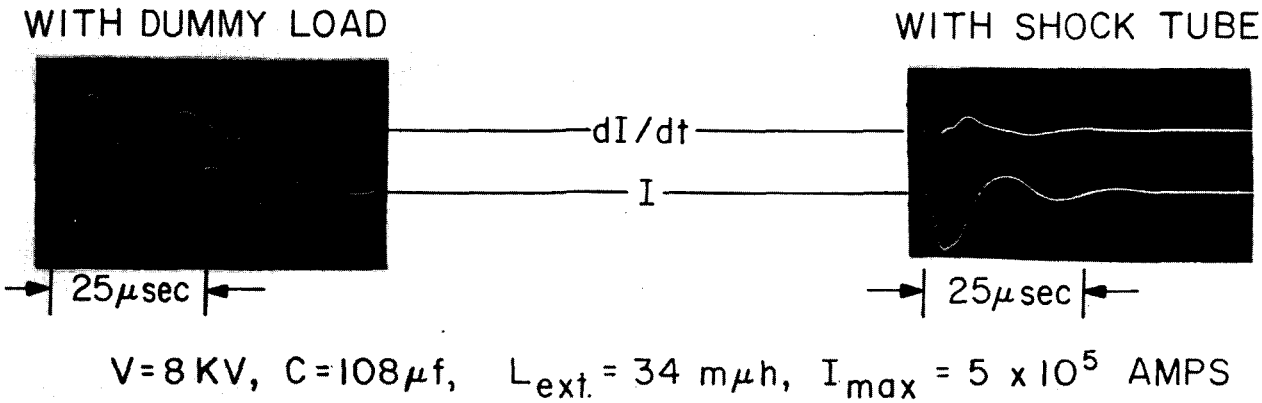

Fig. 2 - Electrical characteristics of the discharge for a dummy load and for the shock tube

of the same material for the arc chamber. Nickel electrodes spaced 22 mm apart were used and sealed in with O-rings. *

In order to eliminate cold layers of absorbing gas between the plasma and the vacuum spectrograph slit, the end of the tube was constructed of nickel-plated brass with the vacuum spectrograph slits installed at the plasma boundary (see Fig. 3). Three ports were provided (not shown on Fig. 3), equipped with quartz windows, for observing the plasma in the visible spectral region (see Fig. 1). A vacuum of 10^{-5} mm Hg was maintained between shots. By the use of a liquid-nitrogen-cooled trap, all harmful impurities, including excessive hydrogen, were removed from the system within a three-minute pumping interval.

Vacuum Spectrograph

The vacuum spectrograph used for this experiment was a McPherson model 240, which was a 2-meter, normal-incidence combination spectrograph and scanning monochromator with a reciprocal dispersion of 3.75A/mm and a measured resolution of 0.06A.† The grating was coated with aluminum and lithium fluoride and subsequently overcoated with a very thin layer of magnesium fluoride for protection against hygroscopic effects (11). The coating had a measured reflectance of 60 percent at Lyman-α and 62.5 percent at Lyman-β. An EMI type 6255B photomultiplier was used with a photoemission-scintillation-type detector (12) to measure the far ultraviolet radiation. The instrument was equipped with an accurate scanning mechanism that allowed the wavelength to be manually set and varied in small increments to a high accuracy.

Auxiliary Spectrographs

Several instruments were used to study the plasma in the visible region of the spectrum during various phases of the experiment. Space-resolved, time-integrated spectra were obtained with a Zeiss quartz prism spectrograph with a reciprocal dispersion of 27A/mm at 4000A and a range of 2050A to 5500A; the shock tube was imaged along the slit.

*The final design included two O-rings per electrode. One was placed about 6 mm inside the tube. It was not greased and served mainly as a cushion for the tube. The second O-ring was placed against the outer rim of the tube and provided the vacuum seal. This design facilitated the quick replacement of tubes without requiring special electrodes for each tube due to nonuniformities in the quartz. Also, the inner split O-ring effectively isolated the vacuum grease from the hot plasma.

†These values refer to a particular 1200 lines/mm grating.

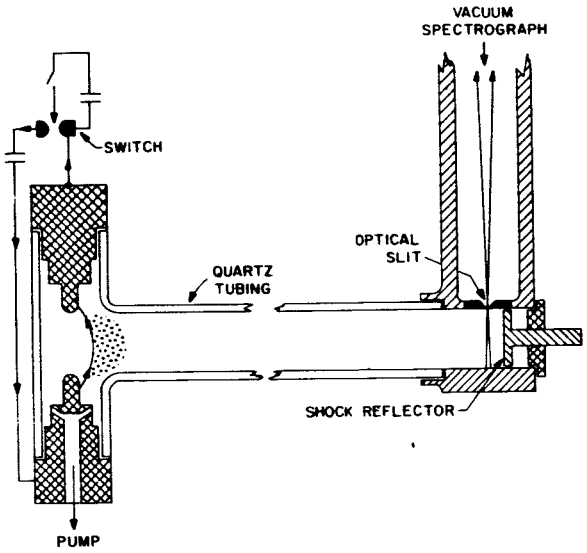

Fig. 3 - T-tube schematic showing the vacuum spectrograph slits

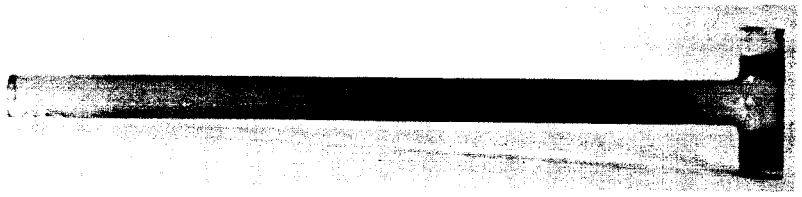

Fig. 4 - A 50-cm shock tube after sixty discharges

Time-resolved spectra in the wavelength region of 4200A to 6500A were provided by a rotating-drum prism spectrograph. This instrument had a reciprocal dispersion of 150A/mm at 5000A and a wavelength resolution of 3.5A. At a writing speed of 0.12 mm/μsec, a time resolution of 10^{-7} sec was obtained.

Two monochromators were employed to measure the electron density and the temperature as functions of time. One was a Leiss double prism instrument, with a reciprocal dispersion of 150A/mm at 5000A, which was used for the density determination. This instrument was calibrated on an absolute scale with a standard tungsten lamp (see Fig. 1) as discussed in the next section. The temperature was measured using Helium-I lines and the nearby continuum with a Bausch and Lomb 500-mm grating monochromator having a reciprocal dispersion of 16.5A/mm.

High-Speed Camera

Measurements of the shock hydrodynamic conditions were made with a streak camera (13), which was an f/2.9 instrument capable of resolving 10^{-8} sec signals at a writing speed of 5.8 mm/μsec. The usual orientation used was with the camera slit parallel to

the tube axis so that the position and velocity of the various interfaces could be determined as a function of time (see Fig. 7). Often, however, image rotators (dove prisms) were placed along the tube to study the planarity of the shock front as a function of time and position along the tube.

Oscilloscopes

A Tektronix 555 dual-beam oscilloscope recorded the electron density (visible continuum radiation) and the vacuum ultraviolet signal simultaneously. It was triggered from the arc by a pickup loop, and the sweeps were delayed (internally) appropriately so that a 5 μsec/cm sweep could be utilized for greater accuracy. An additional Tektronix 551 dual-beam oscilloscope was triggered from the 555 delayed sweep output for the correlated measurements of electron density and temperature.

DESCRIPTION OF EXPERIMENT

Development of the High-Density Source

At the outset of this experiment it was realized that electron densities as high as 10^{19} cm^{-3} might be required to broaden the Lyman-α line sufficiently to permit a detailed study of its complete profile with existing equipment. Thus, the initial phase of the experiment dwelled entirely on the development of a uniform, very high electron density atmosphere for the optically thin layer of hydrogen to be studied. While operation at these extremely high ultimate pressure conditions (~200 atmospheres), with the minute hydrogen concentrations permissible, without introducing too much self-absorption later proved infeasible, these studies did result in a uniform, highly stable, reproducible light source of very low impurity concentration, suitable for accurate scans of the line wings at lower densities.

Magnetic Compression Experiments – Experiments involving magnetic compression machines had shown that a deuterium plasma could be confined in a stable manner at densities up to 10^{17} cm^{-3} at temperatures of 10^6 °K for several microseconds (14). Such a device has certain inherent advantages over arcs or shock tubes as a light source. Since it is an electrodeless system wherein the plasma is kept free from the walls during the times of interest, the impurity level is maintained low, and also the possibility of arcing to a third electrode, such as the vacuum spectrograph slit, is eliminated.

For these reasons, our first approach to the light source problem was with the use of a small magnetic mirror machine operating in the temperature region of 20,000°K. With an existing 20-kilojoule (kj) condenser bank similar to that described in the preceding section, we were able to produce peak currents of 10^6 amperes in 3 μsec in a single-turn coil 15 cm long and 3 cm in diameter, resulting in peak fields of 80,000 gauss at the tube center. A faster bank of 0.3-μf capacitance operating at 28 kilovolts was used to preionize the gas by producing approximately 600 volts/cm circumferentially in the plasma prior to the compression phase.

With initial pressures of 1 mm Hg in helium and argon, a volume compression ratio of 10 was obtained, which resulted in a final electron density of about 3×10^{17} cm^{-3}. This density was verified approximately by time-resolved line profile studies in argon. Ultra-high-speed photographic streak camera studies were also made using a coil consisting of 1-cm sections spaced longitudinally at 1-cm intervals. Typical results, shown in Fig. 5, indicate a very stable plasma for a period of 3 μsec.

It soon became apparent, however, that the high compression ratio desired could not be obtained with the 20-kj bank due to the large amount of field penetration into the plasma

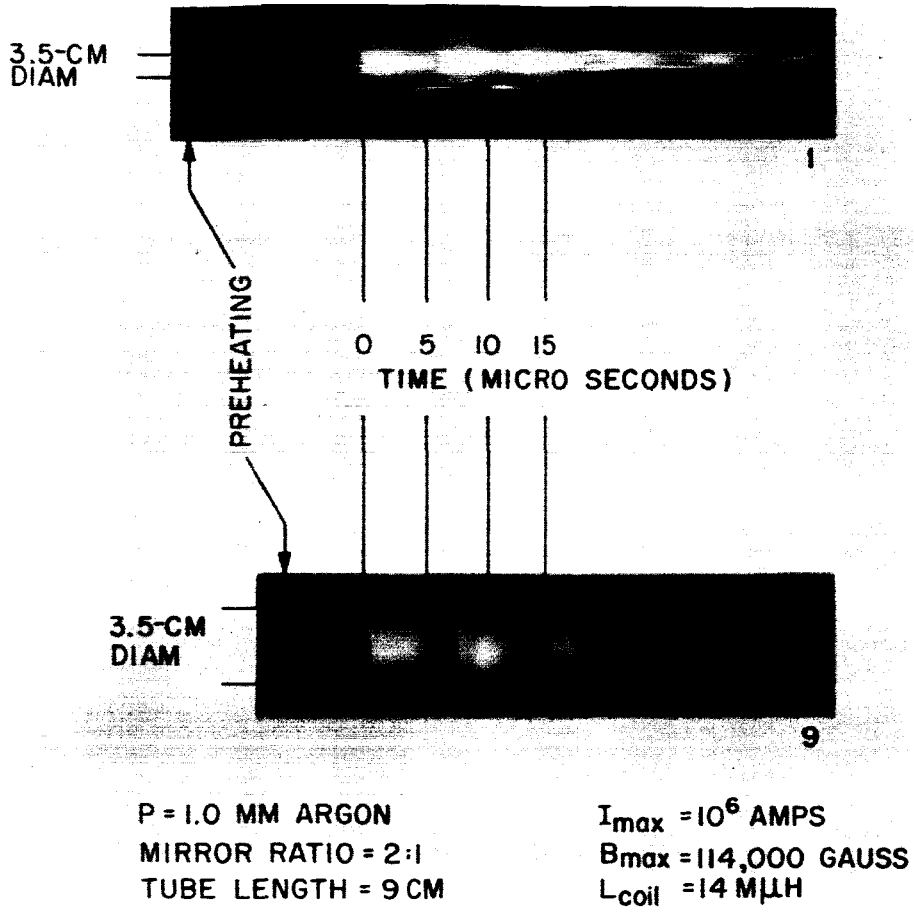

Fig. 5 - Streak photographs of a magnetic compression in argon

before the current reached peak value. This difficulty could only be remedied at these low temperatures either by developing a faster condenser bank or by using a tube of larger diameter, which would require considerably more energy. Since such a condenser bank was not available, and the results of preliminary tests on the electromagnetic linear shock tube were encouraging, the magnetic compression approach was not pursued any further.

H-Tube – Preliminary studies were initiated to explore the possibilities of using a linear electromagnetic shock tube in an H configuration as previously described by Kolb in Ref. 15. In such a device, high-current arcs are formed at each end of a straight tube and the resulting approaching shock waves are allowed to collide at the tube center. Observations with time-integrated and with time-resolved streak camera photography (Fig. 6) indicated that difficulties existed in producing the collision at a given point and also in eliminating arcs down the shock tube. However, these studies did demonstrate the feasibility of generating strong linear shock waves at high initial pressures with the available capacitor bank and encouraged us to proceed to the simple T-type shock tube, equipped with an end reflector, in which the above mentioned problems inherent in the H-tube are eliminated.

T-Tube – The T-type linear shock tube originated with Fowler (16,17) and was later further developed and used by Kolb and others (8,18-20) as a uniform light source for spectroscopic studies on high-temperature plasmas. The efforts of these groups have been toward producing high temperatures at moderate densities in gases of near 100 percent ionization. However, no previous experiments have been directed towards high densities and pressures at low degrees of ionization, as in conventional shock tube studies (9, 21, 22). One result of the present study has been the obtainment of a reasonable

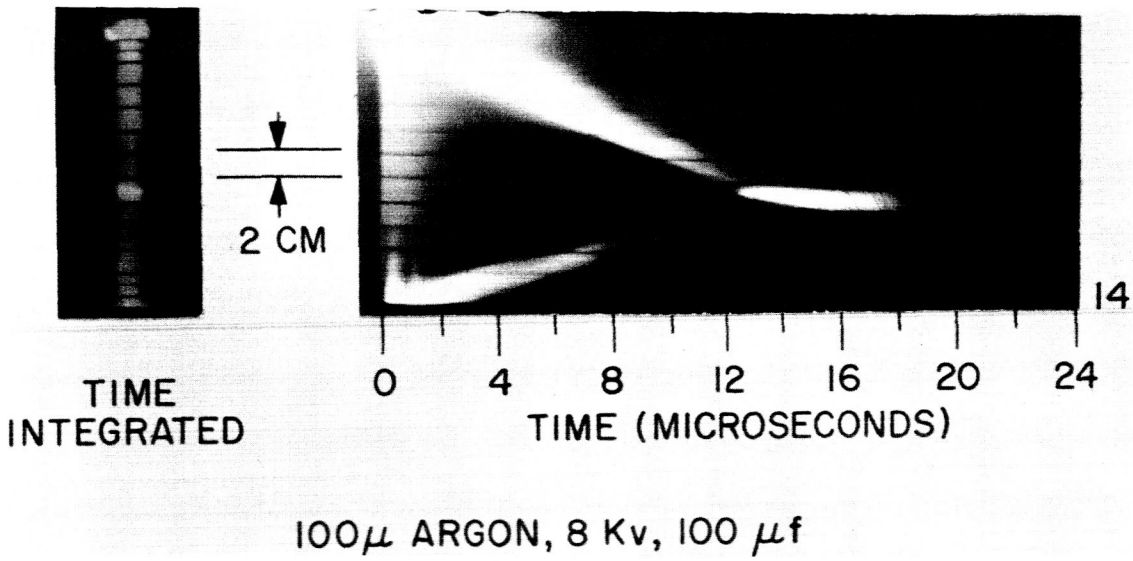

Fig. 6 - Streak photograph study of an H-type shock tube for time-integrated (left) and time-resolved (right) observations

agreement of experimental results with those of conventional shock tubes, as well as with the Rankine-Hugoniot equations.

In developing the shock tube as a light source for this experiment, several criteria were established and upheld throughout the development phase as being fundamental to the success of an accurate experiment:

1. A region must exist behind the reflected shock front that is relatively free from impurities, including hydrogen which may be added in controlled amounts. This is most important in order that a reliable measurement of the absolute intensity of the continuum radiation may be made for use in calculating the electron density (as discussed in the next section). Furthermore, the region used for diagnostics should remain free of impurity deposits on the walls, which could cause a lowering of the wall transmittance when as many as 100 shots are required without cleaning (see Fig. 4).

2. The conditions in the tube must be sufficiently reproducible to permit the accumulation of adequate data in a reasonable time and within the useful lifetime of the tube. Reproducibility is particularly important for vacuum ultraviolet studies since the intensity is so strongly dependent upon source temperature.

3. Likewise, the tube should not break during the number of shots required for a complete profile.

4. The tube must be of transparent material at the point of observation and along the tube for as great a distance as possible to permit streak photographs and space-resolved spectra to be taken.

To satisfy these requirements, a detailed study using streak photography, and both time-resolved and space-resolved spectroscopy, was carried out.

Initial studies with tubes of 15 cm length indicated that the plasma behind the reflected shock wave was dominated by impurities, presumably originating from electrode material and wall and sealant materials. Studies with longer (50 to 75 cm) tubes, however, showed that there exists a separation of fronts in the incident wave similar to that observed in conventional shock tubes, such that a nonluminous shock front is followed by a luminous front, which in turn is followed by a cold layer behind an interface emitting primarily

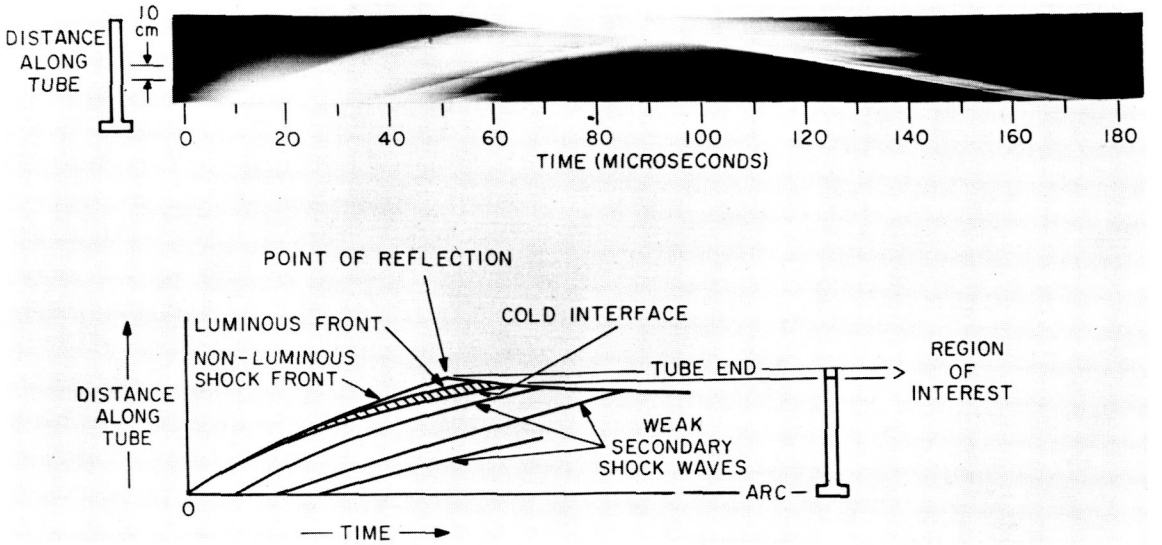

Fig. 7 - Streak photograph of a 75-cm T-tube discharge

impurity radiation. (These regions are illustrated along with a typical streak photograph in Fig. 7.) The separation of these fronts begins at about 40 cm from the arc and increases as the wave progresses along the tube. The relaxation time associated with this separation is most likely due to the relatively low ionization cross section for neutral particle collisions in the shock front vicinity, compared to electron impacts on neutral atoms that occur nearer the luminous front.* Thus, any pre-excitation of particles in the vicinity of the shock front could decrease this separation, and there is a good possibility that precursor radiation in the vicinity of the arc serves to reduce the relaxation time in that region (20).

The reflected shock wave moves into a region of partial ionization created by the incident shock wave. Encounters with the incident luminous front and, subsequently, the incident cold interface tend to destroy the various ordered motions and produce multiple cool fronts traveling back towards the arc region.

The results, as indicated by streak photography taken in color and in black and white (Fig. 7), by time-resolved spectroscopy (Fig. 8), by space-resolved spectroscopy (Fig. 9), as well as by shock tube inspection (Fig. 4), show that:

1. The reflected shock wave is in pure helium with a high continuum intensity due to the high electron density.

2. The incident luminous front is in almost pure helium (some hydrogen is evidenced by the presence of hydrogen Balmer series lines).

3. The highly impure cold interface is turned back at the collision with the reflected shock wave so that the region near the tube end stays free from impurity radiation and wall-darkening effects.

From studies such as these, by varying free parameters such as initial pressure, voltage, and tube length we observed the following limiting conditions.

*Streak photographs taken with an approximate 5-percent hydrogen admixture show a decrease in separation, presumably due to the lower ionization potential for hydrogen, leading to more efficient heating by collisions.

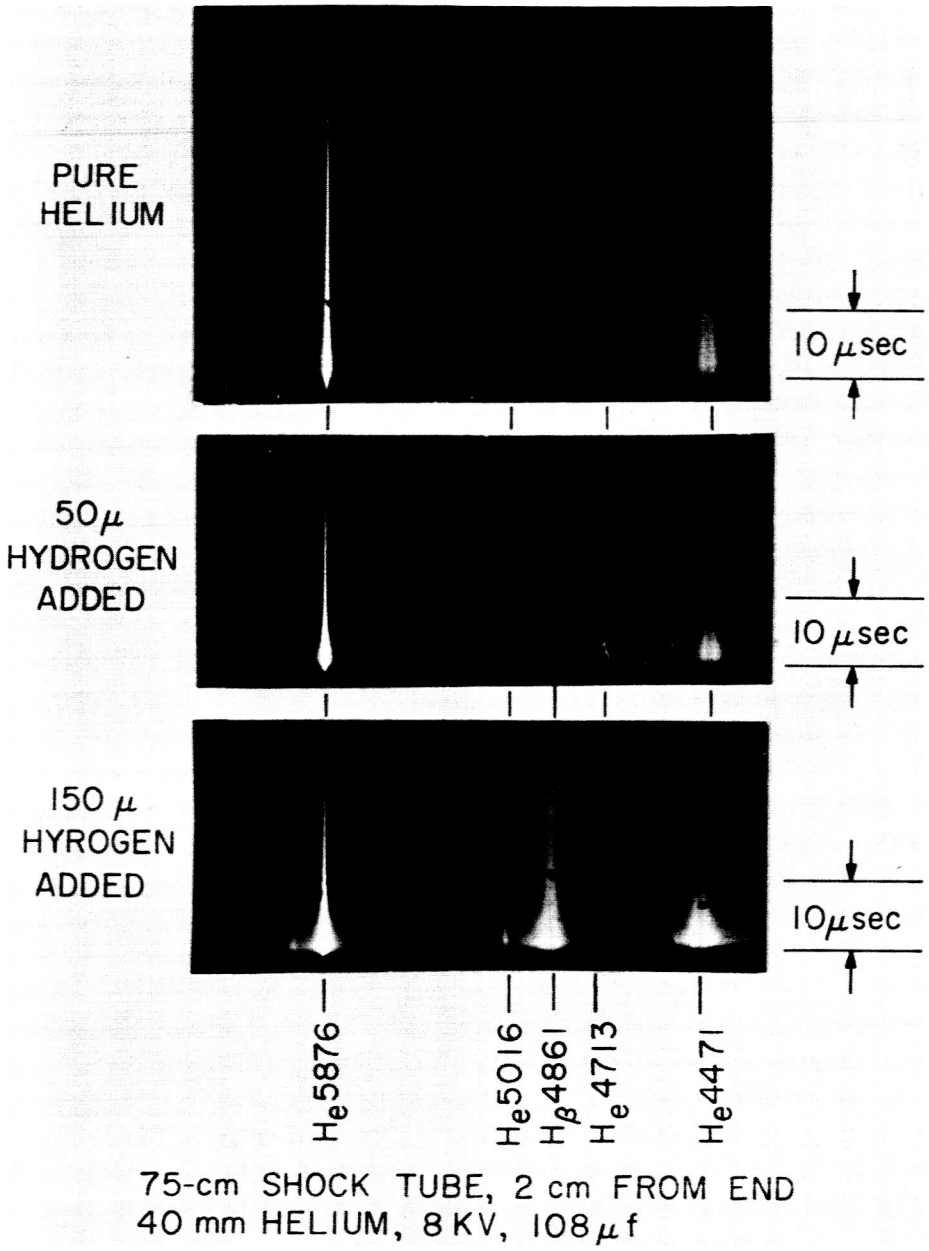

Fig. 8 - Time-resolved spectra taken at 2 cm from one end of a T-tube

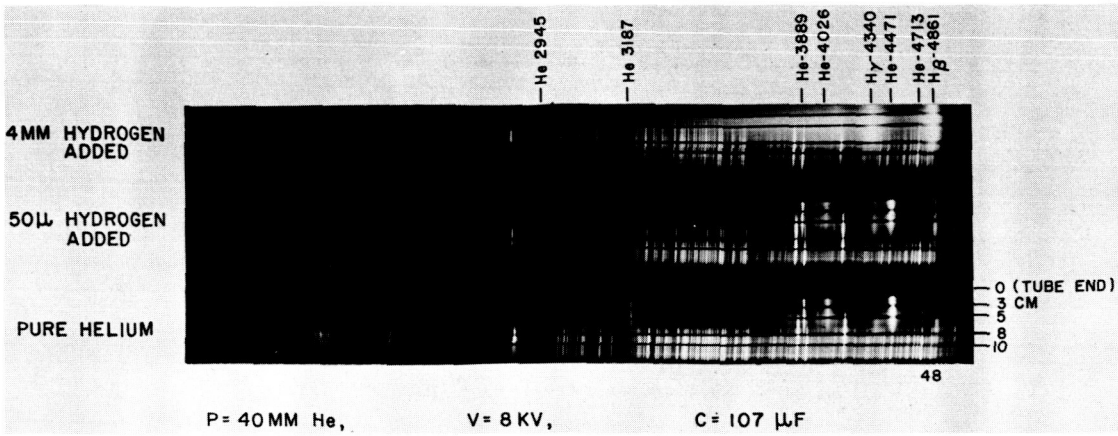

Fig. 9 - Space-resolved spectra taken along the T-tube axis

1. For shock tubes too short in length, the front separation was too small and our working region disappeared, as discussed above. Also, for tubes too long the shock strength decreased to a point at which unreasonable amounts of energy were required to drive the initial shock wave.

2. At low initial pressures (below 20 mm Hg), again, unreasonably high energies were required to obtain sufficient electron densities, and also the separations discussed above decreased. At high initial pressures the separation was satisfactory. However, the particle pressure on the end plate increased until the end piece would blow off or break at about 60 atmospheres.* At very high initial gas pressures this occurs at low electron densities (i.e., low degree of ionization) which is undesirable.

3. One generally tries to raise the voltage to achieve the desired electron density at any pressure, since it is perhaps the easiest parameter to control. Often, however, the associated increase in shock velocity reduces the front separations prohibitively. Also, upper power limits are usually set by the ratings of the capacitor bank and associated components, as well as the strength of the tube material.

With these effects and limitations known, we started with a 20-cm-long shock tube, set the pressure at 30 mm Hg, and raised the voltage until the separation of fronts became too small to provide a reasonable working region. Keeping this maximum voltage, we raised the pressure to regain the separation desired. When this caused the end to break before reaching the desired densities, we increased the tube length and repeated the procedure. The results of these studies indicated that:

1. The tube material found to be most satisfactory was quartz with a wall thickness of 3 mm. Pyrex was found to craze excessively and shattered after a few shots. All other materials used in the tube, including 96 percent pure aluminum oxide, nylon, and Teflon, while withstanding the thermal shocks, decomposed rapidly and required a system cleaning after three firings.

2. The first ten to twenty firings after cleaning a tube always showed a high impurity content, as well as poor reproducibility, and the results were discarded. The cleaning action produced by these initial shots, however, was sufficient to allow usable data to be taken from the subsequent shots (see Fig. 10 for typical reproducibility), with a three-minute pumping period between runs at a vacuum of $\sim 10^{-5}$ mm Hg.

*See Ref. 9, p. 56.

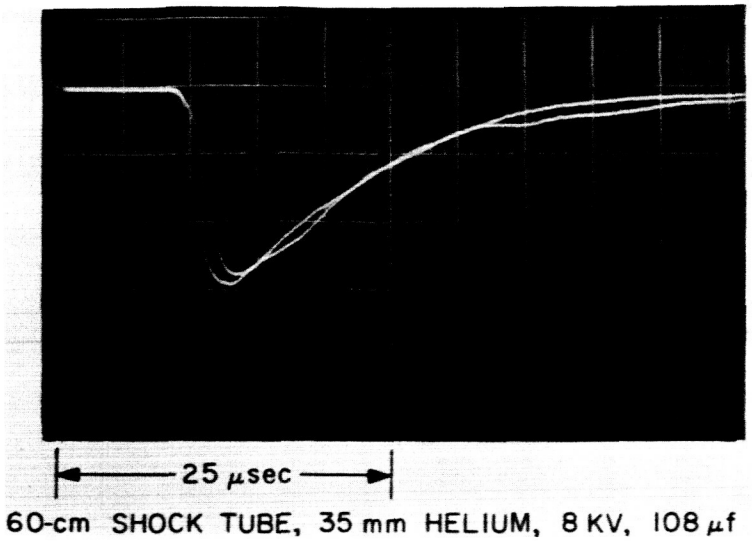

Fig. 10 - Reproducibility of the continuum signals

3. An electron density of 10^{19} cm^{-3} was obtained with no separation of shock and luminous fronts in a 50-cm tube at a pressure of 50 mm Hg and a voltage of 9 kv, while $\sim 4 \times 10^{17}$ cm^{-3} was reached in a 75-cm tube for a 6-cm usable region at 40 mm Hg and 8.1 kv. For the former conditions it was necessary to replace the tube end piece between shots, which is undesirable due to contamination. Also, excessive amounts of hydrogen were included in the luminous zone (see Fig. 9).

4. The relaxation time behind the reflected shock, determined from photomultiplier signals (Fig. 10) and streak spectra (Fig. 8), was found to be less than 1 μsec at the 4×10^{17} cm^{-3} condition and reduced to ~ 0.2 μsec when 0.4 percent of hydrogen was added. Here the lower ionization potential of hydrogen caused an increase in the amount of ionization before the reflected shock wave, without significantly affecting the final state of the plasma in which most electrons are given off by helium atoms.

Vacuum Spectrograph Operation

In coupling a vacuum spectrograph to the experiment, several complications arose. Since the T-type shock tube is an internal electrode device, the vacuum spectrograph represents a third electrode at ground potential when no windows are used. While lithium fluoride does transmit reasonably well down to 1100A, it was found to have a useful lifetime of only a few shots, probably due to surface damage from the plasma.

The presence of this third electrode establishes an alternate current path along the tube axis which can lead to the destruction of the shock wave and ultimate damage to the spectrograph slit. Since the vacuum pumping system is an integral part of such a spectrograph and must normally be coupled to ground through the power lines, it was necessary to float electrically the entire spectrograph above ground. This was accomplished by incorporating an air-core isolation transformer designed for radio tower beacon lighting.* This provided 50,000 volts of insulation, with 32 μμf of coupling capacitance, while transmitting 4000 watts of power at an efficiency of 94 percent.

Finally, the cooling water lines were isolated by using 6 to 8 feet of rubber hose, since the water acts as an insulator for short-time voltage pulses.

*Supplied by Hughey and Phillips, Inc., Burbank, Calif.

Further difficulty in utilizing the vacuum spectrograph with the T-tube was encountered due to the layer of relatively cool gas, at shock tube pressure, between the plasma and the slit. Studies made transverse to this "side arm" showed some excitation of visible hydrogen lines in this region, even when the port was reduced to a 0.5 mm × 5 mm horizontal slit at the plasma. The final solution was to incorporate the slit into the shock tube at the plasma, as shown in Fig. 3 and discussed in the preceding section. There is still evidence of a plasma beam traveling through the slit and striking an internal baffle in the spectrograph (see last section). Also, reliable data on the Lyman-α line showing a wing radiation response to variations in hydrogen concentration, which was consistent with similar visible spectroscopic measurements, was obtained only with an entrance slit greater than 70μ. This implies that there may yet exist some reabsorption behind the slit which may be surmounted by sufficient intensity, i.e., by using an entrance slit of 100μ.

The detector used for the vacuum ultraviolet measurements was of the photoemission-scintillation type (sensitive only below 1300A), developed by Lincke and Wilkerson (12), which consists of a gold cathode at a potential of -15 kv and a nearby plastic scintillator which is coated with a 2000A-thick layer of aluminum to render it opaque to stray visible light but transparent to photoelectrons with energies greater than 3 kev (see Fig. 11). A separate vacuum system was employed to maintain a pressure of 10^{-6} mm Hg at the detector at all times.

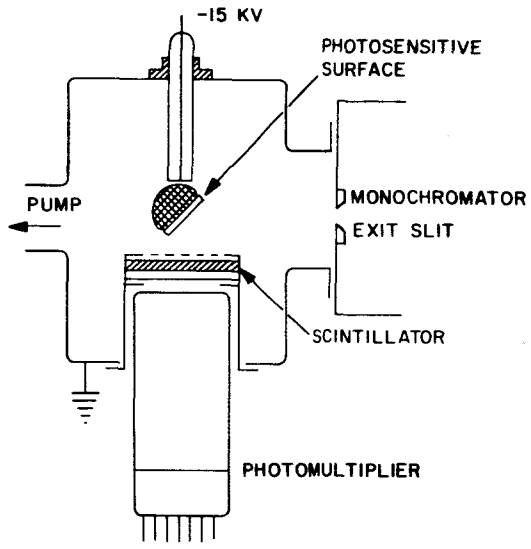

Fig. 11 - Schematic of the photoemission scintillation detector (from Lincke and Wilkerson (12)

Since it is known that oil vapors from vacuum pumps have a deteriorating effect on the special high-reflectance grating coatings, a liquid-nitrogen filled cold trap was installed before the main chamber in the spectrograph.

The ultraviolet data was obtained by filling the shock tube to 47 mm Hg pressure, opening the flap valve at the 100μ entrance slit of the spectrograph, and firing the bank when the pressure reached 40 mm Hg in the shock tube. Between shots during a profile determination, the observed wavelength was shifted over a known interval by accurately timing a calibrated motor-driven gear box and also by means of a calibrated mechanical counter. The calibrations were checked by scanning in similar steps between nearby

lines obtained from an ac capillary discharge tube. Smoothness and reproducibility of the timed phase of the scan was verified by observing a broad mercury line from a static source and scanning the wing of its profile in varying small wavelength intervals. Mechanical errors in reproduciblity of the scan could be maintained at less than 0.002A for a typical 0.25A step, provided that the direction of scan was not reversed.

Auxiliary Spectroscopic Measurements

To obtain the electron density and the temperature in the light source, the energy emitted in separate regions of the visible spectrum was measured using the following techniques.

Density From the Visible Continuum – Determination of the electron density from the visible continuum radiation required a spectral interval both optically thin and free from line radiation so that an accurate measurement of the continuum intensity could be made. To satisfy the condition on the optical depth, operating conditions were sought under which the calculated continuum intensity would be less than 10 percent of the black-body intensity. At a temperature of 20,000°K and an electron density of 4×10^{17} cm^{-3}, the calculated spectral emissivity is approximately 1 percent at 5000A, i.e., well within our set upper limit.

The second condition imposed on the spectral region chosen for this measurement was that any line radiation present be of negligible magnitude. Spectroscopic studies (Figs. 8 and 9) taken with no hydrogen added indicate that broad regions exist in which there is no impurity line radiation present in noticeable amounts. Photoelectric scans over the region of interest verified these results (Fig. 12). Furthermore, at 5160A and 5414A (chosen for our final density measurements), the addition of up to 1 mm of hydrogen has no effect on the continuum intensity.

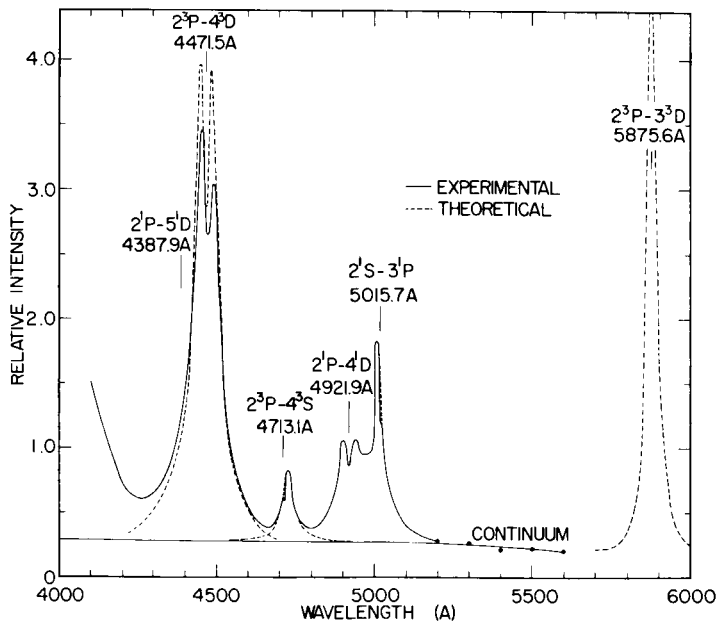

Fig. 12 - Photoelectric scan of the visible helium spectrum

The accuracy of this technique depends critically on the absolute intensity calibration of the monochromator used for the measurement. The calibration was accomplished with a tungsten ribbon lamp whose brightness temperature was determined by the National Bureau of Standards. Calibration of the instrument was based on an in situ technique (8) and was carried out as follows:

1. The photomultiplier current i_S with the shock tube as a source was measured. The slit sizes, photomultiplier voltage, and neutral-density filters were adjusted to give a reasonable signal. Also, the wavelength dial was set below 2000A and the scattered light level was checked and found to be always negligible for the Leiss double prism monochromator.

2. Next, the shock tube was replaced by the calibrated tungsten lamp. By using this in-situ technique, the slit sizes, wavelength interval, solid angle, and surface area all remain the same and cancel out in the comparison of the light emitted from the shock tube to that of the standard source.

3. The photomultiplier current i_L was measured with the tungsten lamp as the source at a known brightness temperature. Here care was taken to assure that the anode current i_L was maintained sufficiently low compared to the dynode bleeder supply current i_B so that less than 1-percent distortion in the tube gain was introduced during the static calibration. For a type 1P28 photomultiplier, this precaution can be shown to be equivalent to assuring that i_L be no greater than 2 percent of i_B. For the pulsed case, when the shock tube is used, capacitors across the last dynodes serve to maintain a constant interdynode voltage during the times of interest.

4. The brightness temperature S, as measured outside the lamp by the National Bureau of Standards, is defined as the temperature of an equivalent blackbody of intensity $[B(\lambda,S)]$ for 6530A radiation. This is related to the true tungsten filament temperature T by

$$\{B(6530,T) \quad \epsilon(6530,T) \quad \tau(6530)\}_{inside} = \{B(6530,S)\}_{outside}. \tag{2}$$

Rutgers and De Vos (23) have presented this as a nomograph of T versus S, using a quartz window transmission factor τ of 0.92 and a value of tungsten emissivity ϵ as measured by De Vos (24).

5. Knowing T from Eq. (2), the intensity I_L at any wavelength λ inside the lamp, i.e., at the filament, may be calculated from

$$I_L(\lambda,T) = \epsilon(\lambda,T)\ B(\lambda,T). \tag{3}$$

6. After determining the transmission factors τ_s and τ_L for the shock tube and for the lamp window, respectively, at the wavelengths used, it is possible to relate the spectral intensity I_S from the ionized gas to the known intensity I_L by

$$\frac{I_S\ \tau_S}{I_L\ \tau_L} = \frac{i_S}{i_L}. \tag{4}$$

7. Since the current i_L is of the order of 15 μa, while i_S is in the milliampere region, we depended heavily on the linearity of the photomultiplier tubes. This was checked with a xenon flash lamp and neutral-density filters using a technique described by McLean et al. (8), which consists of comparing the shape of a reproducible light pulse for different signal levels and noting the point at which distortion sets in.

Temperature from a Line-to-Continuum Ratio – The plasma temperature can readily be determined by the technique of measuring the total intensity of a helium line and the nearby continuum and computing the ratio (18, 25) (discussed in the next section). Complications arise, however, when the electron density is high enough so that the lines overlap seriously, and also when there is excessive absorbing gas near the walls to reabsorb the stronger line radiation generated in the plasma.

Both of the above difficulties occurred in this experiment and caused erroneous results in the temperature measurements obtained initially by total line intensity measurements. For this reason, it was necessary to make a detailed shot-to-shot scan with a scanning monochromator over the visible helium spectrum, as shown in Fig. 12. The theoretical profiles were calculated from the measured electron density and fitted to the experimental curve. Self absorption of strong helium lines in the hot plasma, as well as reabsorption of the cores of the lines by the high concentration of neutral atoms in the boundary layer, is evidenced in the comparison with theory in Fig. 12. Finally, the continuum was measured in a region free from line radiation and extrapolated to the region of the lines of interest, using the continuum theory and the total wavelength response of the detection system.

Since neither the continuum theory nor the line broadening theory are sensitively dependent upon temperature, this measurement of electron temperature was entirely adequate here. However, fluctuations in temperature can greatly affect the experimental vacuum ultraviolet signal levels (i.e., a 10-percent change in T results in a 50-percent change in intensity). Fortunately, the fluctuations in the temperature could be controlled to better than 1 percent during a profile scan by measuring all signals at the instant of some preselected electron density and also by monitoring the transit time of the shock wave to 1 percent (see "Oscilloscopes," in the second section). Fluctuations of 7 percent in N_e correspond to a 1 percent variation in T, while a 1-percent change in velocity results in approximately a 1-percent variation in T under our conditions (9).

SPECTROSCOPIC THEORY

Review of Hydrogen Line Broadening Theory

Before a comparison of the experimental data on the line profiles can be made with the theoretical predictions, we must examine the possible mechanisms contributing to the broadening under our conditions and estimate their relative importance.

An omnipresent source of line broadening is the natural broadening due to the finite lifetime of excited states. This is the sole mechanism for broadening in an atom completely isolated from all other particles and completely at rest. However, in environments normally encountered in thermal light sources, these natural broadening effects (which amount to approximately 10^{-4}A) are completely negligible compared to other damping mechanisms.

If our isolated atom is now allowed to move, a second broadening mechanism enters the picture and is due to the Doppler frequency shift of the emitted radiation from an atom moving with a velocity v. Assuming a Boltzmann velocity distribution for the atoms in motion, a Gaussian frequency distribution function is obtained for the line shape and is given by

$$I(\lambda) = I_o \exp\left(-\frac{c^2(\lambda-\lambda_o)^2 M}{\lambda_o^2 2kT}\right) \tag{5}$$

with a total half-width of

$$\delta\lambda = 2\left(\frac{2\lambda_o^2 kT}{Mc^2} \ln 2\right)^{1/2} \tag{6}$$

where M is the molecular mass and I_o is the central intensity at wavelength λ_o (26). At our conditions of $T \sim 2 \times 10^4$°K, this results in a total half-width of 0.12A for Lyman-α and will produce only negligible effects for $\Delta\lambda > 0.2$A when folded into the total Stark profile.

Now assume that our moving atomic radiator is placed in the vicinity of other particles, both charged and neutral. A third mechanism for broadening sets in. This mechanism, called pressure broadening by Lorentz (27) in his pioneering work on line broadening, is due to particle collisions in which the line width is proportional to the frequency of collisions and, thereby, to the pressure. We may further subclassify the pressure broadening mechanism into (a) that due to foreign (different quantum states) atoms or molecules where the interaction potential V goes as r^{-6}, r being the distance between the perturber and the radiating atom; (b) that due to resonance or interchange effects caused by similar (same quantum state) atoms where $V \sim r^{-3}$, and (c) that due to Stark effect broadening caused by charged ions or electrons where $V \sim r^{-2}$ for the linear Stark effect. Since hydrogen exhibits a large linear Stark effect in the electric field of the perturbers, this mechanism will dominate the pressure broadening contribution to our measured profiles of hydrogen lines.

As it is not the intention in this report to enter into a detailed review of pressure broadening of spectral lines, only a brief resume will be given here, with emphasis placed on the efforts pertaining to hydrogen lines. Several review articles exist (28-30), and an extensive review of the earlier work pertaining to hydrogen lines in particular is given by Kolb (31).

We may further classify the Stark broadening theories by identifying those dealing with (a) impact perturbations, where the approximation is made that the average time between collisions is much greater than the average collision duration time, or that the average collision only causes small effects, and (b) those dealing with perturbations due to quasi-static fields whose distribution is found by averaging the static fields over all possible charged particle configurations.

The impact theory approach was initiated by Lorentz (27) in 1906. He assumed complete destruction of the coherence of radiation when a normally unperturbed wave train is interrupted by collisions. Improvements on the Lorentz approach were made by Lenz (32) and by Weisskopf (33), who made allowances for finite phase shifts in the emitted radiation. However, their consideration fails to account for broadening due to a succession of weak collisions since they do not consider as effective any collisions producing phase shifts less than some arbitrary value of order unity. Lindholm (34) and Foley (35) succeeded in removing this deficiency.

The quasi-static approach to Stark broadening was initiated in 1919 by Holtsmark (36). Spitzer (37) in 1939-1940 sought to synthesize these two approaches and succeeded in showing that they follow from the same general formalism. He also showed that collision-induced (nonadiabatic) transitions can contribute to impact broadening. However, his results are limited to binary collisions and also neglect the effect of electron collisions.

Anderson (38) in 1949 made a more complete study, including the nonadiabatic effects, for completely degenerate (i.e., no splitting) initial and final states and applied this to lines in the microwave and infrared regions. However, his work is also limited to binary collisions for the electrons. The adiabatic and nonadiabatic effects of electron broadening

in hydrogen were considered in 1955 by Margenau, Bloom, and Kivel (39) who used the Born approximation but neglected the ion field splitting of the degenerate hydrogen lines. Kolb (31) emphasized the need of a unified theory to adequately account for the simultaneous broadening due to electron impacts and the quasi-static effects of the slower moving ions. However, his results were limited to the wings of the hydrogen lines.

Thus, a general theory was still lacking which could account simultaneously for the quasi-static splitting into Stark components (ions) and the further broadening by adiabatic (phase shifts) and nonadiabatic (induced transitions) electron impacts. A combination of a generalized impact theory developed by Kolb and Griem (4) and independently by Baranger (3) with the quasi-static theory corrected for correlation and shielding effects was presented by Griem, Kolb, and Shen (5) and by Mozer (6). The splitting of the degenerate levels due to the slowly moving ions is described by a quasi-static theory using a Holtsmark-type distribution function. Then the simultaneous broadening of each Stark component and transitions among them due to electron collisions are included through the use of an impact theory based on the classical path assumption for the motion of the electrons. The theory has been worked out in detail for the case of completely degenerate initial and final states and also for the case of a nondegenerate ground state, when the broadening arises only from perturbations of the upper state. This latter case obviously corresponds to the Lyman series of hydrogen.

Further stimulus for the experimental investigation of the profiles of these lines stems from the very nature and simplicity of the Stark effect for Lyman-α and Lyman-β. To clarify this remark, we recall that hydrogen exhibits the unique properties of completely degenerate energy levels. These levels result in a large linear Stark effect that makes higher order effects negligible and, in a certain sense, simplifies the theory considerably. Characteristics of specific lines also prove to be very interesting. For example, Lyman-α exhibits, in a static field, two unshifted Stark components and two shifted ones, such that a measurement of the shape of the line core could help resolve the electron broadening effects on the unshifted components. On the other hand, the core of Lyman-β, in which all components are shifted in a static field, shows a central dip, the shape of which depends critically upon the ion field distribution function used. Unfortunately, a detailed experimental study of these central zones was made impossible by the reabsorption of the line core by hydrogen in the cooler boundary layers (see section on "Data, Analysis, and Results").

Turning to the line wings, we have first the simple Holtsmark function in which the intensity falls off asymptotically as $\Delta\lambda^{-5/2}$. The more recent calculations which include the electron broadening effects give wing formulae (40) for various regions which approach the Holtsmark limit near the line center but diverge rapidly as $\Delta\lambda$ increases until reaching twice the Holtsmark result in the extreme wings. This maximum divergence occurs at relatively small values of $\Delta\lambda$ for the narrow Lyman series lines, i.e., before different lines overlap, allowing true profiles over three orders of magnitude in intensity to be obtained. By sliding the theoretical curves on a logarithmic ordinate scale, a comparison of theories for Lyman-α shows a gain of ~ 3 for the complete theory as compared to the Holtsmark theory in the far wings (see Fig. 14). Thus we are able to verify the additional effect of the electrons on the far wings of the resonance lines by accurately measuring the slope of the profile. This is particularly interesting for the Lyman-α line since its very simple structure (only two displaced Stark components) inherently lends itself to a most accurate and sensitive application of the theoretical techniques used for other lines from higher levels, where typically as many as 22 components are involved (e.g., for H_β at 4861A).

Electron Density Determination from the Visible Continuum Radiation

Determinations of plasma electron density and temperature, independent of line broadening theory, may be obtained from absolute and relative intensity measurements,

respectively, in optically thin regions. Values of electron density and temperature are required in order to compare the experimental results for the line profiles with the theoretical predictions.

For the density measurements, the continuum intensity is measured at a wavelength at which the source is optically thin and free from line radiation. The continuous absorption coefficient for hydrogenic atoms was originally derived by Kramers and is given by (41)

$$k_\nu = \left(\frac{2B_1}{B_o}\right)\left(\frac{16\pi^2}{3\sqrt{3}}\right)\left(\frac{Z^2e^6kT}{c\ h^4\nu^3}\right) \exp\left(-\frac{Ry}{kT}\right)\{F\}_H \tag{7}$$

where

$$\{F\}_H = \left\{\sum_{n'>n_c}^{\infty} \frac{2Ry}{kT}\left\langle\overline{g_{fb}(n')}\right\rangle_\ell \frac{\exp(\Delta E_{n'}/kT)}{n'^3} + \overline{g_{ff}}\right\}_H \tag{8}$$

for an isolated hydrogen atom, and

k_ν = absorption coefficient per neutral atom whose density is N_o

$\Delta E_{n'}$ = I.P. - $E_{n'}$ (= Ry/n^2 for hydrogen)

$\left\langle\overline{g_{fb}(n')}\right\rangle_\ell$ = mean free-bound Gaunt factor averaged over the sublevels of level n'

$\overline{g_{ff}}$ = mean free-free Gaunt factor

$B_1(T)$ = ion partition function

$B_o(T)$ = neutral atom partition function.

The Gaunt factors used above have been calculated (42), and n_c is defined as the quantum number of the lowest state that contributes to the free-bound radiation at a given wavelength. This may be determined by the lowest value of n satisfying $\Delta E_{n_c} \lesssim hc/\lambda$.

Within the brackets ($\{F\}_H$) the summation term represents the free-bound contributions to the continuum absorption coefficient, while the last term represents the free-free part for an isolated atom. Due to the blending of discrete states of high quantum numbers into a continuum upon interaction of the atom with microfields in the plasma, the summation is terminated at some n_g and continued as an integral contribution (26). Thus,

$$\sum_{n'>n_c}^{\infty} \frac{2Ry}{kT}\left\langle\overline{g_{fb}(n')}\right\rangle_\ell \frac{\exp \Delta E_{n'}/kT}{n'^3} \tag{9}$$

becomes

$$\sum_{n'>n_c}^{N_g} \frac{2Ry}{kT}\left\langle\overline{(g_{fb}\ n')}\right\rangle_\ell \frac{\exp(\Delta E_{n'}/kT)}{n'^3} + \overline{g_{ff}} \exp\left[\frac{Ry}{(n_g+1)^2kT}\right] - 1 . \tag{10}$$

Saha's equation may be written as (26)

$$\frac{N_i N_e}{N_o} = \frac{2B_1(T)}{B_o(T)} \left(\frac{(2\pi mkT)}{h^3}\right)^{3/2} \exp\left(-\frac{I-\Delta I}{kT}\right), \tag{11}$$

where $I-\Delta I$ is the lowered ionization potential as discussed recently, e.g., by Griem (43), and N_i and N_e are the total number densities of ions and electrons per cm^3, respectively.

Substitution of Eq. (11) into Eq. (7) yields

$$k_\nu = \frac{N_i N_e}{N_o} C \exp\left(-\frac{\Delta I}{kT}\right) \frac{Z^2 c^2}{2h\nu^3\sqrt{kT}} \{F\}_H, \tag{12}$$

where

$$C = \frac{32\pi^2 e^6}{3\sqrt{3}\, c^3 (2\pi m)^{3/2}} = 6.36 \times 10^{-47} \qquad \text{[c.g.s. units]}.$$

One now multiplies with N_o, the depth of the emitting layer ℓ, and the Kirchoff-Planck function corrected for induced emission, namely,

$$B_\nu = \frac{2h\nu^3}{c^2}\left(1-\exp\left(-\frac{h\nu}{kT}\right)\right)\Big/\left(\exp\left(\frac{h\nu}{kT}\right)-1\right) \tag{13}$$

$$\equiv \frac{2h\nu^3}{c^2} \exp\left(-\frac{h\nu}{kT}\right),$$

and obtains the intensity ϵ_ν

$$\epsilon_\nu = k_\nu N_o \ell B_\nu = \frac{N_i N_e Z^2 C \ell}{\sqrt{kT}} \{F\}_H \exp\left(-\frac{\Delta I}{kT}\right). \tag{14}$$

Since all energies are measured from the ionization limit, this hydrogen calculation can also be used for neutral helium provided that we make the following corrections.*

First, since for neutral helium the excited electron does not see a closed shell core, an effective nuclear charge of $Z-S$ is required to account for the screening effect of the second electron. However, for $n \gtrsim 3$ we can assume (44) that $S = 1$ and $Z_{eff} = 1$.

Second, to account for the noncoulomb nature of the true wavefunctions for helium, we may introduce n^* as the effective quantum number, defined by (45)

$$I_{He} - E_{n,\ell} = \Delta E_{n,\ell} = \frac{Ry}{(n^*)^2} \tag{15}$$

*The corrections described in Eqs. 15 through 17, which essentially modify $\{F\}_H$ resulting in $\{F\}_{He}$ for the helium case, are based somewhat on intuition. For the present conditions the resulting $\{F\}_{He}$ is about 10 percent higher than $\{F\}_H$. More recent computations of effective helium Gaunt factors based upon quantum defect calculations of bound-free ionizing cross sections, which are formally much more satisfying, are now being completed and will be described in detail in a forthcoming book entitled "Plasma Spectroscopy" by H.R. Griem (McGraw-Hill). Preliminary results of these computations indicate an excellent agreement with the calculations described here.

or

$$(n^*)^2 = \frac{I_H}{I_{He} - E_{n,\ell}} . \tag{16}$$

Since the helium levels are not degenerate in ℓ, we must modify the factor $\{F\}_H$ used above accordingly:

$$\{F\}_{He} = \left\{ \frac{2Ry}{kT} \sum_{n^* > n_c}^{n_g} \frac{1}{2n^2} \sum_{\ell=o}^{n^*-1} (2J_{n^*,\ell} + 1) \frac{\overline{g_{fb}(n^*,\ell)}}{n^{*3}} \exp\left(\frac{\Delta E_{n^*,\ell}}{kT}\right) + \overline{g_{ff}} \exp\left(\frac{Ry}{(n_g+1)^2 kT}\right) \right\}_{He} . \tag{17}$$

Finally, we can set $N_i = N_e$ since the degree of second ionization in helium is negligible at our temperatures (8,18). Equation 14 then becomes

$$\epsilon_\nu = \frac{N_i N_e C \ell}{\sqrt{kT}} \{F\}_{He} \exp\left(-\frac{\Delta I}{kT}\right), \tag{18}$$

From this, ϵ_λ is obtained by

$$|\epsilon_\lambda| = \frac{c}{\lambda^2} \epsilon_\nu \left[\frac{\text{ergs}}{\text{sec-cm}^3\text{-steradian}}\right]. \tag{19}$$

The only factor still undetermined here is n_g, the principle quantum number of the last discrete state. n_g is determined by the amount by which the series limit is apparently lowered due to the broadening of higher series lines into a pseudocontinuum. Several attempts have been made towards computing this quantity. These have recently been reviewed by Griem (43), who concludes that the approach of Inglis and Teller (46) is probably the most dependable. Their results give

$$N_e n_g^{15/2} = 0.027\ a_o^{-3} \tag{20}$$

or

$$\log_{10} n_g = \frac{23.26 - \log_{10} N_e}{7.5} \tag{21}$$

where

$$a_o = \hbar^2/me^2 . \tag{22}$$

It should be noted that the value of $n_g \sim n_g + 1$ is not at all critical in determining the electron density.

Finally, we might note that the above expression for finding N_e from ϵ_λ is very insensitive to temperature in the vicinity of 20,000° K (18), with a 10 percent variation in temperature producing only a 1 percent variation in N_e for a given ϵ_λ.

Temperature Determination from a Line-to-Continuum Ratio

An accurate measurement of the temperature in helium may be obtained below 30,000 °K by determining the intensity of an optically thin neutral helium line relative to the underlying continuum (18). If we consider an emission line originating from a

quantum transition m to n, the associated total line absorption coefficient k^{ℓ} (integrated over frequency) is given by

$$k^{\ell} = k_{\nu}^{\ell} d\nu = \frac{\pi e^2}{mc} \frac{N_o g_n}{B_o} f_{abs} \exp(-E_n/kT) \tag{23}$$

where f_{abs} is the absorption oscillator strength for the transition, g_n is the statistical weight for level n, and the other quantities are as defined in the above subsection.

Using Kirchhoff's law, we can define the ratio of intensities K' as

$$K' = k^{\ell}/k_{\nu}^{c} .* \tag{24}$$

Taking k_{ν}^{c} from Eqs. (12) and (17) and using Eq. (23) above, we have for K'

$$K' = \frac{\pi h^4 e^2}{mc(2\pi m)^{3/2} CkT} \frac{g_n f_{abs}}{B_1} \frac{\exp(\Delta E_n/kT)}{\lambda \Delta\lambda} \{F\}_{He}^{-1}. \tag{25}$$

Taking B_1 equal to 2, we get

$$K \equiv K'\Delta\lambda = (0.672 \times 10^5) \frac{g_n f_{abs}}{\lambda T} \exp\left(\frac{\Delta E_n}{kT}\right) \{F\}_{He}^{-1}. \tag{26}$$

The oscillator strengths have been tabulated (47), and K has been correctly plotted versus T for three prominent neutral helium lines by Berg, et al. (18).†

This method therefore consists of measuring the total line intensity, subtracting off the measured continuum level, and taking the ratio of this result to the continuum intensity.

DATA, ANALYSIS, AND RESULTS

The data obtained from this experiment (48) and used for the profile determinations was time-resolved and obtained from photographed oscilloscope traces (e.g., Fig. 10) and streak camera film (Fig. 7). For a given shot, all the data used was read coincidently in time at an instant of preselected constant electron density, as monitored by the visible continuum intensity.

Obtainment of the Vacuum Ultraviolet Data

The data used for the profile determinations in the vacuum ultraviolet region was obtained from a wavelength scan of approximately 100 discharges. Approximately

*While this simple derivation from absorption coefficients requires equilibrium population of the lower level, in truth only the upper level must be so populated for application of the technique to temperature measurement.

†The curve for 5016A in Berg's article (Ref. 18, Fig. 1) is erroneous and should be recalculated using Eq. (26) above.

twenty shots were executed initially, without scanning, in order to discharge-clean the shock tube; after this cleaning, sufficient reproducibility was obtained to permit a shot-to-shot scan. Most of the high-frequency noise from the photomultipliers was integrated out electronically.* However, for very weak photomultiplier signals, random cathode statistical noise "spikes" on the oscilloscope traces introduced uncertainties which were reduced by repeating such shots prior to resuming the scan procedure.

The scan was begun on the short-wavelength side of the line center and continued to wavelengths beyond the line center until the signal reached a constant background level (see Fig. 13). Since some saturation at high intensities was indicated, due to self-absorption of the broad line in the plasma, as well as a narrow-band reabsorption at the line center by cooler gas in the boundary layer, the next step was to intentionally add hydrogen in known amounts and to measure the resulting intensities at various fixed wavelengths (e.g., at -1A and +4A, as well as 0A) from the center of Lyman-α in order to determine the saturation level. (This also served to determine the magnitude of the omnipresent† background hydrogen level in the shock tube.) Then the scan was repeated over one wing with the hydrogen content increased in order to obtain better accuracy on the far wings of the line where the signal approaches the background level. Following this the background signal level was measured at several points far removed from the line on each side of the line. Finally, several random points on the profile were repeated to check against any systematic deviations occurring throughout the data run.

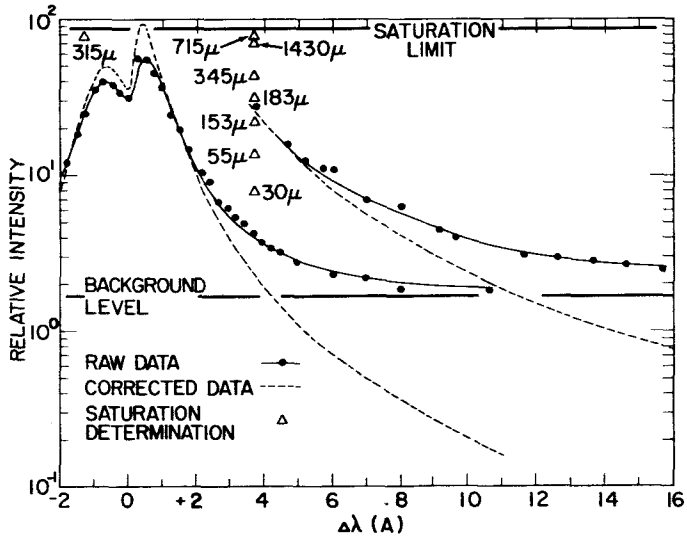

Fig. 13 - Data for the Lyman-α line profile

Reduction of Data

The first correction to be applied to the raw data was the subtraction of the background level, which results mainly from scattered light.‡ This level is determined from measurements made at wavelengths far removed from, and on each side of, the line center. A

*Electromagnetic noise from the discharge itself was negligible since the transit time of the shock wave is ~50 μsec, after which time the arc current is damped out (Fig. 2).

†Since mass-analyzed spectroscopically pure helium was used, with an impurity level less than four parts per million, this hydrogen was presumed to originate in the shock tube materials.

‡An estimate from measured and theoretical emissivities indicates that the background radiation consists of ~90 percent scattered light of other wavelengths and ~10 percent continuum at the wavelength of the line.

further check on the validity of this measurement, which is obtained at a low signal level, is afforded by use of the second profile obtained at higher hydrogen concentration. After subtracting the expected background contribution from all signals, as discussed above, the ratio of measured signals between the two wing profiles at discrete wavelengths is calculated. This ratio should be independent of wavelength for a constant hydrogen concentrations during each scan. However, any slight errors in the background level show up as increasingly large variations in the resultant ratio as $\Delta\lambda$ increases, with the predominant effect occurring in the lower-hydrogen-level scan results. Thus, any systematic variations that occur in the ratio between profiles, as the wavelength increases, may be used to obtain more accurate values for the background correction.

The second correction to be applied to the raw data accounts for self-absorption of the emitted radiation in the plasma. Assuming that we are dealing with a uniform plasma in thermal equilibrium, radiative transfer theory gives for the change in intensity dI_ν across a layer of thickness $d\ell$

$$dI_\nu = k'_\nu B_\nu d\ell - k'_\nu I_\nu d\ell, \tag{27}$$

where the first term describes the emission from the layer and the second describes the absorption in the layer. Here B_ν is the Planck function, I_ν the intensity incident on the slab, and k'_ν the absorption coefficient corrected for induced emission, where

$$k'_\nu = k_\nu \, [1 - \exp(-h\nu/kT)]. \tag{28}$$

The solution of Eq. (27) for our conditions results in

$$I_\nu = B_\nu \, (1 - e^{-\tau}), \tag{29}$$

where τ is defined by

$$\tau \equiv k'_\nu \ell. \tag{30}$$

If one neglects all self-absorption, i.e., assumes the second term in Eq. (27) is zero, the solution becomes

$$\int dI_\nu = \tau B_\nu, \tag{31}$$

which is the "optically thin" solution.

Our correction procedure therefore consists of measuring the ratio of I_ν to B_ν (obtained from the measured saturation limit) and computing τ from Eq. (29). The product τB_ν from Eq. (31) then gives the equivalent optically thin intensity.

The practical accuracy of this second correction depends upon our determination of the true saturation limit, while the theoretical validity depends upon whether or not such a limit is truly the blackbody limit at the plasma temperature. We may obtain theoretical support here by starting with the line absorption coefficient as given for the Lyman lines by

$$k'_\nu = \frac{2\pi e^2}{mcB_o} Nf \; [1 - \exp(-h\nu/kT)] \; S_\nu(\nu), \tag{32}$$

where N is the total neutral-hydrogen atom density, f is the absorption oscillator strength, B_o is the neutral-atom partition function, and S_ν is the shape function defined (49) such that $\int S_\nu d_\nu = 1$. We may obtain N from Saha's equation (Eq. (11)) written as

$$\frac{N_e N_p}{N} = \frac{2B_1}{B_o} \frac{(2\pi mkT)^{3/2}}{h^3} \exp[-(I - \Delta I)/kT], \tag{33}$$

where N_e is the total electron density in the plasma, N_p is the proton density, and $B_1 = 2$. If we now define N_H and N_{He}, respectively, as the total hydrogen and helium atom densities prior to the discharge, we have

$$N_H \; [N_e/(\alpha \; N_{He})] = N_p + N, \tag{34}$$

where α is the degree of ionization of the helium.* Since everything on the left side in Eq. (34) is known, we may eliminate N_p from Eq. (33) by using Eq. (34) and then substitute Eq. (33) into Eq. (32) to eliminate N. The result is an expression for τ.

$$\tau = k'_\nu \ell = \tau(N_H, \nu, T), \tag{35}$$

which can be used with Eq. (29) to compute the expected spectral emissivity $\epsilon = I_\nu/B_\nu$ at any wavelength.

By plotting τ versus N_H for $\Delta\lambda = +4A$ and comparing the curve with the data taken with various hydrogen concentrations at the same wavelength and temperature, we were able to estimate the background hydrogen content (~15 microns) in the tube for each data run as well as the true† saturation signal limit. Using this value for N_H we were able to compute ϵ from Eqs. (29) and (35) and compare it with the measured values. The results (see below) substantiated our assumptions used in the data correction within experimental errors.

Results and Error Estimates

The results of a typical data run on the Lyman-α line plotted at an electron density of 3.3×10^{17} cm^{-3} are shown in Fig. 14 where the theoretical curve,‡ according to more recent calculations which include the electron effects on the Stark broadening, is compared with the older Holtsmark quasi-static theory. The theoretical curves are made to fit at the point of equal slope near $\Delta\lambda = 1A$ so that a clear comparison of the wing slopes could be made. The error flags represent a ±8-percent uncertainty in the raw data, i.e., before background and saturation effects were removed. The central dip is due to

*From Saha's equation for helium.

† For large hydrogen concentrations the hydrodynamics and, therefore, the temperatures, etc., were affected in such a manner that an additional effect entered (see Ref. 21, p. 108). Thus curve fitting as described here was necessary to obtain the true limit.

‡The theoretical curves do not include the Doppler broadening which does not contribute significantly for $|\Delta\lambda| > 0.2A$.

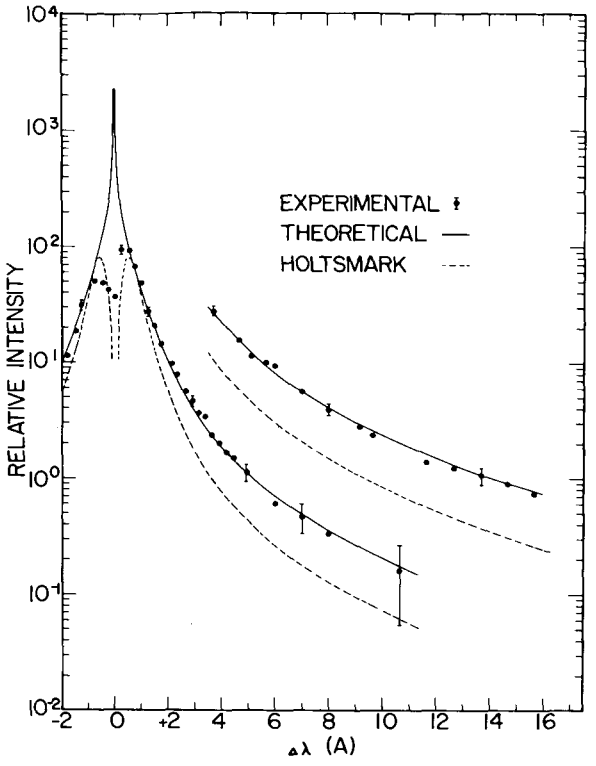

Fig. 14 - Comparison of the Lyman-α results with recent theory and with the older Holtsmark quasi-static theory

reabsorption of the line core by the cooler plasma in the boundary layer, as has been verified by negative results obtained in seeking an increase in signal with added hydrogen in this region. A shift of the line towards the red is indicated by the increased peak intensity on the high-wavelength side of the central dip. This has also been observed in time-integrated film studies and is probably due to higher order Stark effects, since the first-order effect is completely symmetrical.

The peak electron density, as determined from the visible continuum radiation and averaged over a ±10-percent maximum shot-to-shot fluctuation in the eighty shots used for this profile, was $(3.6 \pm 0.4)10^{17}$ cm^{-3}. The estimated error (~10 percent) in N_e here results from uncertainities of ~20 percent in the continuum intensity I_c, as calculated from the formula for continuum radiation, Eq. (18), where $I_c \propto N_e^2$ and, thus, $\Delta N_e/N_e \propto \Delta I_c/2I_c$. This ~20-percent uncertainty reflects the cumulative effects on I_c of uncertainties in the hydrogen-like formula used (~5 percent), the temperature measurement (~8 percent), the intensity standard (~3 percent), and the technique used in obtaining and analyzing the data (~10 percent).

Likewise, the temperature, as determined from a line-to-continuum ratio measurement in the visible region (Fig. 12), gave $T = (20.5 \pm 1.6)10^3$°K, with the error here resulting from uncertainties in the ratio K' (Eq. (24)) of 25 percent due to effects of the approximate hydrogen-like continuum formula used (~5 percent), the oscillator strength value (~5 percent), as well as the measurement of the line-to-continuum ratio signals (~15 percent).

The spectral emissivity of Lyman-α at $\Delta\lambda = +2$A, as found experimentally (see "Reduction of Data" p. 23), was $\epsilon = 0.10 \pm 0.02$, while the value obtained by calculation

(see Eqs. (32) through (35)) resulted in $\epsilon = 0.09 \pm 0.06$, with the large error here due mainly to the temperature measurement (~8 percent) which reflects as a ~50-percent uncertainty in ϵ. Errors in other parameters, such as N_e (~10 percent), S_ν(~10 percent), and ℓ (~5 percent), also contributed.

Because of the difficulty with boundary layer reabsorption in the region $\Delta\lambda < 0.5$A, as experienced with the Lyman-α line, our major incentive in studying the Lyman-β line was to check the techniques used for Lyman-α. Since Lyman-β is considerably weaker, it was necessary to add 40 microns of hydrogen for the first profile scan and then to increase the hydrogen to 200 microns for the auxiliary scan. The final results for Lyman-β, plotted at an electron density* of $N_e = 3.0 \times 10^{17}$ cm^{-3} over the range -6A to +6A, are shown in Fig. 15. For $\Delta\lambda > +6$A the signal was quite erratic due to impurity lines, which in most cases were correlated with known lines of silicon and oxygen. These lines served as a further check on the accuracy of the scanning procedure utilized for Lyman-α. Also, the experimental value for the emissivity was consistent with that calculated from the plasma conditions, as was the case for Lyman-α.

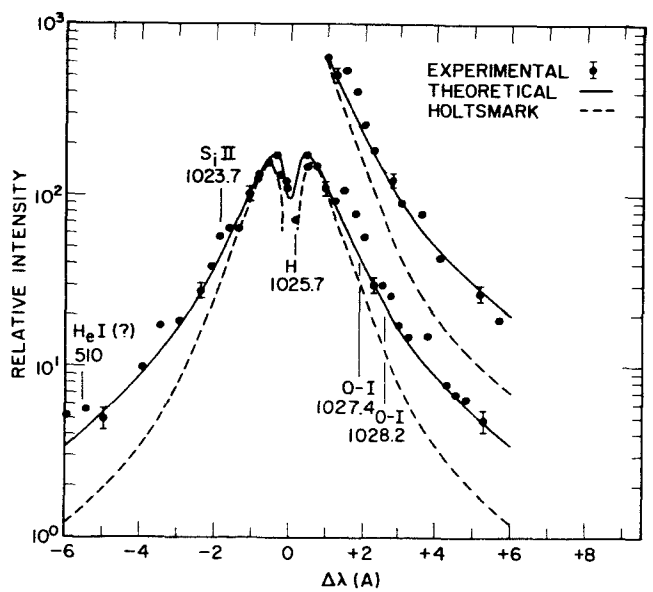

Fig. 15 - Comparison of the Lyman-β results with recent theory and with the older Holtsmark quasi-static theory

The present results for Lyman-β suggest a slight shift of the line towards shorter wavelength, as evidenced by the appearance of the reabsorption dip due to boundary layer reversal at ~0.2A above the center of the emission line.†

Finally, we have the auxiliary quantitative hydrodynamic measurements obtained with high-speed streak photography (e.g., Fig. 7). Using the calculations by Seay (9) on the

*The measured average peak electron density here was $(3.45 \pm 0.3)10^{17}$ cm^{-3}

†Preliminary studies on the Lyman-β line with higher resolution (~0.25A) indicate that the reabsorption problems may not be as serious as those encountered in the Lyman-α line study. Therefore, a more detailed study of the core of the Lyman-β line is being conducted at the present time. Further results will be included in a forthcoming publication by the author and H.R. Griem.

Rankine-Hugoniot equations relating the measured incident shock velocity to temperature, electron density, etc., one obtains $T = (20.0 \pm 1.0)10^3$ °K and $N_e = (4.8 \pm 1.9)10^{17}$ cm^{-3}. Comparison of this temperature with that from the spectroscopic measurements indicates that precursor radiation effects, as observed in low-pressure T-tubes (8,50), are not significant under the conditions in this experiment.

SUMMARY, CRITIQUE, AND CONSIDERATION OF FUTURE EXPERIMENTS

The data obtained from this experiment supports the validity of the techniques used in recent calculations (5,6,49) of Stark broadening of spectral lines, where the effect of the electron impact broadening is included with the quasi-static ion broadening. In particular, the results pertain to a single line (Lyman-α of hydrogen) whose wing shows a strong sensitivity to the electron broadening, i.e., the change in slope culminates in a gain of ~ 3 over the purely quasi-static ion broadening theory when the two theoretical profiles are fitted at equal slope near the line center.

Subsequent measurement of the profile of the Lyman-β line provided added confidence in the analysis techniques used for Lyman-α and also provided an independent check on the scanning accuracy through the inclusion of nearby silicon and oxygen impurity lines which, quite fortunately, were not observed near Lyman-α.*

Auxiliary spectroscopic measurements in the visible region made possible the monitoring of electron density and temperature simultaneous with the vacuum ultraviolet signal so that a constant value of electron density could be used throughout the profile plot. In addition, measurements of the shock velocity, combined with the usual Rankine-Hugoniot equations, gave results in close agreement with the spectroscopic results, indicating a lack of significant precursor radiation effects for such a high-pressure T-type shock tube.

During the course of this experiment, several special techniques had to be developed. One involved rebuilding the front of the vacuum spectrograph to combine the entrance slits with the shock tube wall so that the slits were directly at the plasma boundary. This was necessary in order to eliminate the extended regions of cooler gas which tended to reabsorb the emitted radiation from the plasma. Also, considerable time and effort were spent in developing a shock tube and in designing a vacuum seal and mounting arrangement that would withstand the high impulse developed at the pressures involved.

Since determination of the hydrogen background concentration, as well as the saturation limit, was necessary for a proper analysis of the signal resulting from radiation emitted from the near-optically-thick layers near $\Delta\lambda = 0$, a technique using vacuum needle valves was developed for adding hydrogen in known amounts before filling the tube with helium.

In measuring the velocity of the nonluminous shock wave with a streak camera, a mirror was added beyond the transparent reflector of the shock tube such that the camera also recorded the instant of shock reflection. This point in time, along with the known position of the reflector, established the point of reflection on the streak photograph to which the shock front could be extrapolated from the luminous zone nearer the arc (see Fig. 7). This served to define the incident shock velocity at an instant just prior to reflection.

*The He-II line at 1215.17A was estimated to be $\sim 10^{-5}$ times the intensity of Lyman-α under our conditions.

Several phenomena observed in this experiment still remain somewhat unresolved. For example, the acoustical noise level is very high (almost painful) when quartz or pyrex shock tubes are used. However, aluminum oxide tubes are completely quiet (except for switch noise, which is minor) as also are quartz and pyrex tubes that are taped. Some study of this effect indicates that radiation is causing excitation of the external air resulting in an external shock wave, but just what type of radiation is responsible is still undetermined.

Also, there remains the question of the effect of the entrance slit width on the Lyman-α wing signal. With a slit 25 μ wide no effect was observed upon adding hydrogen until ~ 200 microns were added, although simultaneous measurements on Hβ in the visible region indicated that for this measurement only ~15 microns was present initially. For a slit width > 70 μ the results at Lyman-α are consistent with those at Hβ, indicating a broadband absorption effect occurring between or behind the slit jaws.

Associated with the above problem may be another phenomenon observed which involves some sort of a beam that has a tendency to deposit a carbon image of the slit on a lucite plate placed in the optical path inside the vacuum spectrograph. This beam is highly collimated when observed at a distance of 15 cm from the slit, as, evidenced by the obtainment of a clear unattenuated image of a copper screen placed 5 cm from the slit for diffusing the beam. However, at 1 m from the slit no image is observed. Most likely the pressure drop from the slit to the pumping port (at 1 m) causes the ultimate beam diffusion; thus differential pumping behind the slit may be required.

Finally, there is the question of the source of background hydrogen that remains constant throughout the data run of ~100 shots (after ~20 shots initially) in spite of periodic intentional additions of hydrogen in large amounts. This stable hydrogen background was measured to be equivalent to ~15 microns initially in the tube. However, the spectroscopically pure helium used was analyzed with a mass spectrometer and found to contain less than four parts per million of hydrogen, or < 0.16 micron. Therefore, we must assume that the major contribution comes from shock tube materials, such as the walls themselves.

Once the above phenomena are better understood, it would be desirable to extend this work to include, first of all, a more detailed study of the core of the Lyman-β line to learn more about the proper ion field distribution function to be used in the theoretical calculations. A more accurate temperature determination would permit the use of the shock tube as an intensity calibration light source for the vacuum ultraviolet region by producing near-blackbody radiation from homogeneous layers of controlled optical depth. Such a calibration could conceivably be extended to other discrete wavelengths by the addition of other impurity gases, again in controlled amounts.

ACKNOWLEDGMENTS

The author wishes to express his gratitude to Professor H.R. Griem for suggesting the study of the Lyman lines of hydrogen and for his continued guidance and encouragement, to Dr. A.C. Kolb for his stimulating suggestions and support, and to Mr. J.L. Ford for his invaluable technical criticism and assistance. The help, advice, and support received from my colleagues in the Radiation Division, as well as from Mr. W.R. Hunter and Mr. D.W. Angel of the Atmosphere and Astrophysics Division of the U.S. Naval Research Laboratory, are gratefully recalled.

REFERENCES

1. Griem, H., Z. Physik 137:280 (1954)
2. Bogen, P., Z. Physik 149:62 (1957)
3. Baranger, M., Phys. Rev. 111:481 (1958)
4. Kolb, A.C., and Griem, H., Phys. Rev. 111:514 (1958)
5. Griem, H.R., Kolb, A.C., and Shen, K.Y., Phys. Rev. 116:4 (1959)
6. Mozer, B., Ph.D. thesis, Carnegie Institute of Technology, Pittsburgh, Pennsylvania (1960)
7. Kolb, A.C., Phys. Rev. 107:345 (1957)
8. McLean, E.A., Faneuff, C.E., Kolb, A.C., and Griem, H.R., Phys. Fluids 3:843 (1960)
9. Seay, G.E., "The Visible Radiation from Helium in a Strong Shock Wave," Los Alamos Scientific Laboratory Report No. LAMS-2125, June 1957
10. Lupton, W.H., "Fast Triggered Spark Switches For a Two Megajoule Bank," Proceedings Fifth International Conference on Ionization Phenomena in Gases, Munich 1961, Amsterdam:North-Holland Pub. Co., 1962
11. Angel, D.W., Hunter, W.R., Tousey, R., and Hass, G., J. Opt. Soc. Am. 51:913 (1961)
12. Lincke, R., and Wilkerson, T.D., Rev. Sci. Instr. 33:911 (1962)
13. Brauer, F.L., and Hansen, D.F., J. Opt. Soc. Am. 49:421 (1959)
14. Kolb, A.C., "Proceedings of the Second United Nations International Conference on the Peaceful Uses of Atomic Energy," 31:332 New York:United Nations, 1958
15. Clauser, F.H., "Symposium of Plasma Dynamics," Reading, Mass.: Addison-Wesley, 1960, p. 206
16. Fowler, R.G., Goldstein, J.S., and Clotfelter, B.E., Phys. Rev. 82:879 (1951)
17. Fowler, R.G., Atkinson, W.R., and Marks, L.W., Phys. Rev. 87:966 (1952)
18. Berg, H.F., Ali, A.W., Lincke, R., and Griem, H.R., Phys. Rev. 125:199 (1962)
19. Wiese, W., Berg, H.F., and Griem, H.R., Phys. Rev. 120:1079 (1960)
20. Wiese, W., Berg, H.F., and Griem, H.R., Phys. Fluids 4:250 (1961)
21. Turner, E.B., "The Production of Very High Temperatures in the Shock Tube with an Application to the Study of Spectral Line Broadening," AFOSR TN 56-150, ASTIA Document No. AD 86309, Univ. of Mich. Eng. Res. Inst. Report and Ph.D. thesis (1956)

22. Resler, E.L., Lin, S.C., and Kantrowitz, A., J. Appl. Phys. 23:1390 (1952)

23. Rutgers, G.A.W., and De Vos, J.C., Physica 20:715 (1954)

24. De Vos, J.C., Physica 20:690 (1954)

25. Griem, H.R., "Plasma Spectroscopy," Proceedings Fifth International Conference on Ionization Phenomena in Gases, Munich 1961, Amsterdam:North-Holland Pub. Co. 1962

26. Aller, L.H., "Astrophysics; the Atmospheres of the Sun and Stars," New York:Ronald Press, 1953

27. Lorentz, H.A., Proc. Amst. Acad. 8:591 (1906)

28. Weisskopf, V., Z. Physik 34:1 (1933)

29. Margenau, H., and Lewis, M., Revs. Mod. Phys. 31:570 (1959)

30. Baranger, M., "Spectral Line Broadening in Plasmas," Chapter 13 in "Atomic and Molecular Processes," edited by D.R. Bates, New York:Academic Press 1962

31. Kolb, A.C., "Theory of Hydrogen Line Broadening in High-Temperature Partially Ionized Gases," AFOSR-TN-57-8, ASTIA Document No. AD 115-040, Univ. of Mich. Eng. Res. Inst. Report and Ph.D. thesis, 1957

32. Lenz, W., Z. Physik 25:299 (1924)

33. Weisskopf, V., Z. Physik 75:287 (1932)

34. Lindholm, E., Arkiv Mat. Astron. Fys. 32A (No. 17) (1945), 18 pp.

35. Foley, H.M., Phys. Rev. 69:616 (1946)

36. Holtsmark, J., Ann. Physik 58:577 (1919)

37. Spitzer, L., Jr., Phys. Rev. 55:699 (1939); 56:39 (1939); 58:348 (1940)

38. Anderson, P.W., Ph.D. dissertation, Harvard University, 1949; Phys. Rev. 76:647 (1949)

39. Kivel, B., Bloom, S., and Margenau, H., Phys. Rev. 98:495 (1955)

40. Griem, H.R., Astrophys. J. 136:422 (1962)

41. Unsöld, A., "Physik der Sternatmosphären," 2nd ed., Berlin:Springer-Verlag, 1955

42. Karzas, W.J., and Latter, R., Rand Corp., Report RM-2010-AEC (1957), and RM-2091-AEC (1958), Astrophys. J. Suppl. No. 55, VI:167 (1961)

43. Griem, H.R., Phys. Rev. 128:997 (1962)

44. Goldberg, L., Astrophys. J. 90:414 (1939)

45. Bates, D.R., and Damgaard, A., Phil. Trans. Roy. Soc. (A) 242:101 (1949)

46. Inglis, D.R., and Teller, E., Astrophys. J. 90:439 (1939)

47. Trefftz, E., Schluter, A., Dettmar, K.H., and Jörgens, K., Z. Astrophys. 44:1 (1957)

48. Elton, R.C., and Griem, H.R., "Stark Profile Measurement of the Lyman-α Line of Hydrogen," Proceedings of Fourth Annual Meeting Division of Plasma Physics of the American Physical Society, Atlantic City, 1962

49. Griem, H.R., Kolb, A.C., and Shen, K.Y., "Stark Broadening of Hydrogen Lines in Plasma," NRL Report 5455, Mar. 1960; see also NRL Report No. 5805

50. McLean, E.A., Kolb, A.C., and Griem, H.R., Phys. Fluids 4:1055 (1961)